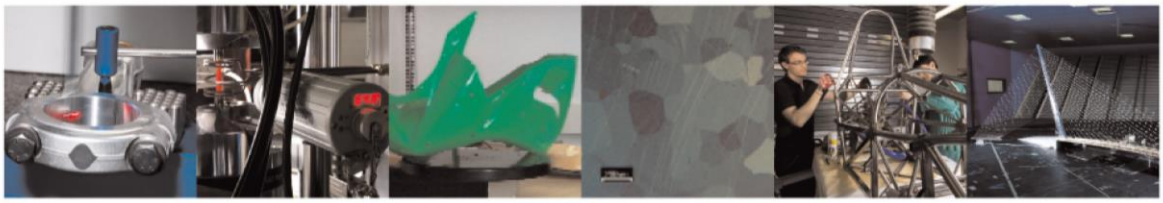

Understanding the effects of temporal waveform modulation of the laser emission power in laser powder bed fusion: Part I - Analytical modelling

Caprio, L.; Demir, A. G.; Previtali, B.

This is a post-peer-review, pre-copyedit version of an article published in JOURNAL OF PHYSICS D. APPLIED PHYSICS. The final authenticated version is available online at: http://dx.doi.org/10.1088/1361-6463/ac984c

Understanding the effects of temporal waveform modulation of the laser emission power in Laser Powder Bed Fusion – Part 1: Analytical modelling

Leonardo Caprio[1]*, leonardo.caprio@polimi.it,

Ali Gökhan Demir[1], aligokhan.demir@polimi.it

Barbara Previtali[1], barbara.previtali@polimi.it

[1]Department of Mechanical Engineering, Politecnico di Milano, Via La Masa 1, 20156 Milan, Italy

*Corresponding author

Understanding the effects of temporal waveform modulation of the laser emission power in Laser Powder Bed Fusion

Leonardo Caprio[1]*, Ali Gökhan Demir[1], Barbara Previtali[1]
[1]Department of Mechanical Engineering, Politecnico di Milano, Via La Masa 1, 20156 Milan, Italy
* Corresponding author

Abstract

The architecture of contemporary fiber laser sources enables users a wide choice in terms of spatial and temporal profiles during the Laser Powder Bed Fusion (LPBF) process. Given the range of possibilities, the need for analytical modelling approaches to predict the consequences of waveform modulation in terms of both thermal and fluid-dynamics aspects over the powder bed, process dynamics and resulting part quality is of great interest. Within the present investigation a moving point source analytical model was developed to study the effect of temporally modulated laser beams over the temperature distribution and recoil pressure induced over the molten region during single track LPBF depositions. This study configures as the first part of an investigation on the topic presented with the aim of developing the modeling framework to predict the effects of temporal waveform modulation in the LPBF process.

The model developed was implemented numerically to simulate the single track LPBF deposition of stainless steel AISI316L with different waveform shapes ranging from the conventional Square Wave emission to Ramp Up, Ramp Down and Triangle waveforms. Modulation at different amplitude levels and different waveform frequencies were also investigated. Results show that temperature variations followed the temporal profile of the power exposed over the material. Consequently, recoil pressure oscillations over the melt region exhibited a periodic profiles correlated to the waveform modulation of the laser power indicating that melt flow may be controlled by means of such techniques. Peak values of recoil pressure, which might be symptomatic of melt pool instabilities, could be reduced employing higher levels of modulation frequency or lower oscillation amplitudes between non-zero values of emission power.

Keywords:

Additive Manufacturing; Laser Powder Bed Fusion; Waveform; Modulation; Analytical model; Recoil pressure

List of Symbols

Symbol	Name	Units
a_n	Coefficients of the Fourier series	-
b_n	Coefficients of the Fourier series	-
c_p	Specific heat capacity	J/kg·K
d_0	Beam waist diameter	µm
f_w	Waveform frequency	kHz
k	Thermal conductivity	W/m·K
k_b	Boltzmann's constant	J/K
l_t	Layer thickness	µm
L_v	Latent heat of vaporization	J/kg
m	Mass per atom	kg
M^2	Beam quality factor	-
n	Order of the Fourier series	-
p_0	Ambient pressure	
P_{avg}	Average laser emission power	W
P_{bk}	Background power of laser emission	W
P_{max}	Maximum emission power	W
P_{pk}	Peak power of laser emission	W
p_r	Recoil pressure	MPa
r	Radial distance from origin of coordinate system	µm
S	Auxiliary solution	-
Si	Simon's number	-
SR	Spatial resolution	µm/pixel
T	Generic temperature field under waveform emission	°C
t_0	Generic starting time instant	µs
T_{amb}	Ambient temperature	°C
T_{CW}	Temperature field under CW emission	°C
t_{exp}	Exposure time of CMOS camera	µs
t_{fall}	Laser fall time	µs
t_i	Specific time instant	µs
$t_{illumination}$	Exposure time of illumination light	µs
$T_{liquidus}$	Liquidus temperature	°C
t_{off}	Laser off period	µs
t_{on}	Exposure time	µs
$t_{response}$	Response time of laser source	µs
t_{rise}	Laser rise time	µs
T_s	Surface temperature of the liquid	°C
$T_{solidus}$	Solidus temperature	°C
t_{tot}	Waveform period	µs
v	Scan speed	mm/s

Symbol	Name	Units
x,y,z	Coordinate system positioned with the moving heat source	µm
α	Thermal diffusivity	m^2/s
β_r	Recondensation factor	-
δ	Duty cycle	-
ΔH_v	Enthalpy of phase transition	J
ΔP	Waveform amplitude	W
η	Process efficiency	-
λ_w	Spatial wavelength of the process	µm
ω_w	Angular frequency of the waveform emission	rad/s
ϕ	Solution to the time-dependent problem	-

1 Introduction

Laser Powder Bed Fusion (LPBF) is an Additive Manufacturing technology which relies on the localised fusion and rapid resolidification of a powder bed after the scanning of a laser beam to achieve the multi-layer deposition of complex freeform objects[1]. Considering the increasing need of digitalised production methods and the requirements for flexible manufacturing of customised high value components, LPBF has been increasingly adopted throughout the industrial scenario[2–4]. As all manufacturing technologies, LPBF possesses different strengths and weaknesses with regards to conventional production cycles also depending on the specific application case[5]. As with all emerging techniques there is still margin for improvement considering recent developments in the fiber laser technology (the most commonly employed source in industrial LPBF systems)[6]. Novel generation laser sources enable modulation of the laser beam in both the spatial and temporal profiles with unprecedented flexibility[7,8]. As reviewed by Demir *et al.*, a transition from CO_2 laser sources to Nd:YAG systems with low beam quality in terms of both propagation and temporal response and eventually to high brightness fiber laser sources, with beam quality factor comparable to Gaussian diffraction-limited levels ($M^2 \approx 1$), power levels beyond 100 W and beam waist diameters in the order of tens of microns, has enabled the industrialisation of LPBF manufacturing systems [9]. Modulation of the laser emission is typically obtained by variation of the emission power from a zero background level up to the peak emission power for a certain duration, with typical square waveforms. The effect of these modulation strategies in LPBF has been extensively studied by Mumtaz *et al.*[10–12] beyond pioneering work by O'Neill *et al.*[13,14]. The use of square wave emission has been investigated by Caprio *et al.* both through analytical and experimental investigations[8,15]. Further experimental research on the effect of pulsed wave emission in LPBF has been carried out by Biffi *et al.* and Wilson-Heid *et al.*[16,17]. The different laser emission modes alter the volumetric deposition rate and precision as well as the mechanical behaviour of the material due to different thermal history during the solidification. A compromise must be sought between the achievable build rate (typically higher with continuous wave emission) with respect to a greater accuracy obtainable with modulated emission[15]. Another aspect which must be considered when employing temporally modulated beams is that the modification of the thermal history of a material, especially in

the case of crack susceptible materials, can alter the defect formation mechanisms eventually avoiding them as shown in the work by Zhang *et al.* for the laser welding of an aluminium alloy[18]. Such techniques are thus of great interest to increase the range of alloys processable by means of LPBF. For instance, the complementary use of pulsed and continuous wave emission was explored by Demir *et al.* to avoid the formation of overheated regions [19]. Pore formation dynamics in pulsed wave LPBF have been further investigated via high-speed X-ray transmissive videography by Hojjatzadeh *et al.* [20].

Although thorough investigations on such topics have been conducted, recent developments in laser technology show that continuous wave fiber lasers may be modulated at high frequency (≥10 kHz) with novel waveforms beyond the conventional square wave[21–23]. Last generation fiber laser sources present rise and fall times in the μs which are thus negligible with respect to the shapes imposed to waveforms which are typically in the order of tens or hundreds of μs. It is thus possible to program the novel laser emission waveforms through the direct programming of the laser pumping diodes or via modulation of the laser analog signal. Such approaches may be beneficial in a wide range of applications ranging from surface structuring to welding [24–28]. Hence, the possibility of enhancing the features of the manufacturing tool thus yields the need for a framework to promote a fundamental understanding of the underlying interaction mechanisms thus providing the means to manipulate the process according to different requirements. In LPBF, the use of novel waveforms can be beneficial to control melt flow via the melt pool oscillations [29]. Such approach can provide the means for a more regular surface finish as well as improving the build rate. With a broad range of emission temporal profile possibilities, the means for modelling tools become of great importance. From this perspective it is essentially important to understand the relationship between the laser emission temporal profile, the temperature field, and the resultant recoil pressure acting on the melt pool.

Analogously to different laser-based processes which have been investigated by the scientific community, the laser-material interaction is identified as a key aspect in determining the process stability and successful production of manufacts in LPBF. In recent years, the scientific community has demonstrated the use of complex high fidelity thermo-fluid dynamic models to study such phenomena. Early examples of such models developed by the

scientific community may be found in the works by Khairallah *et al.* on the description of the physical mechanisms occurring during the process and Xia *et al.* who investigated the effect of hatch distance during the deposition of IN718[30,31]. On the other hand, at the expense of greater inaccuracies, analytical models provide the means to predict the effects of process parameter variations at a fraction of the computational expense. The reasons to why analytical models, especially in the field of laser material processing, are still of great importance for the scientific are discussed by Dowden [32]. Although such modelling efforts have been carried out to understand different aspects of the LPBF process, the influence of the temporal power profile requires further attention.

Accordingly, in the present work an analytical point source model (previously derived by Simon *et al.*) was used to estimate the temperature distribution generated by a time-varying power input during a single-track LPBF of AISI 316 stainless steel [33]. The model was further developed and by using the estimated temperature fields it was possible to estimate the recoil pressure variations induced by a temporally modulated laser beam and predict its effect over the melt pool. The analytical framework was implemented numerically employing different waveform parameters in terms of frequency and amplitude as well as shapes in order to provide a comprehensive outlook on the possibilities introduced by temporally modulated beam in the LPBF. The model proved to be a time-effective solution for a comparative assessment between different waveforms and was used to provide descriptive parameters from the recoil pressure variations as a means for evaluating the performance of different waveforms in LPBF. This manuscript configures as the first part out of two of an extended investigation on the topic. The second part of the research, deals with the results of the experiments conducted to validate the model presented in the present paper and is reported in a separate publication.

2 Modelling of the recoil pressure with periodic laser emission waveforms

Under the effect of a temporally modulated power emission we can expect the melt pool to assume an oscillatory behaviour correlated to the frequency of the power waveform given as an input to our dynamical system. The model hypothesis is thus that the recoil pressure may be considered as a forcing input which commands the oscillatory motion of the molten liquid. A temporally modulated power input will generate a time varying temperature field. Recoil pressure will thus be generated in regions of the melt where the surface temperature will exceed the vaporization temperature of the material thus generating a time varying pressure field over the molten liquid which will cause an oscillatory behaviour. A fundamental hypothesis for the model formulation is that thermos-capillary and viscous forces may be considered negligible with respect to the forcing input, whereas the recoil pressure is fully countered by the surface tension. A schematic representation of the cause-effect relationship of the analytical model is reported in Figure 1 whilst in the following sections the model derivation is explained.

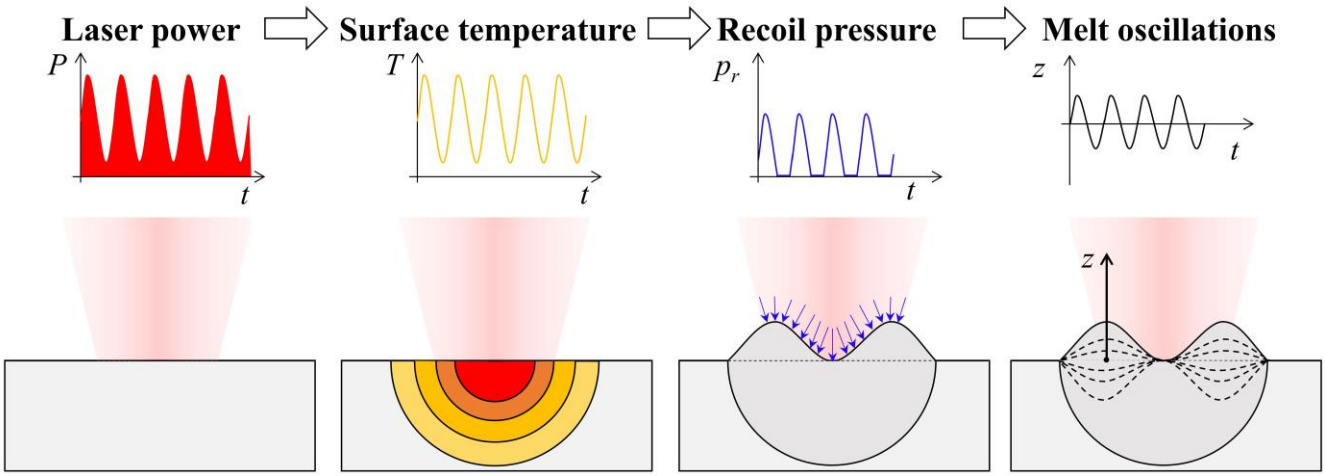

Figure 1. Schematic representation of the cause-effect relation of the analytical model developed

2.1 Laser waveform parameters

The parameters employed to define the temporal modulation waveforms are hereby detailed. When employing modulated laser emission for the LPBF process, the conventional pulsation mechanism implemented rely on a logical on/off temporal emission profile since they are typically activated by [34]means of the digital modulation

signal (schematic representation shown in Figure 2). The power emission profile in the temporal domain is defined by a peak power level P_{pk} which is active for a given exposure time or pulse duration t_{on}. The laser emission is then switched off for a period of time corresponding to t_{off}. Hence, the overall period of one cycle is defined as t_{tot} and may be calculated as the sum of these two periods of time:

$$t_{tot} = t_{on} + t_{off} \tag{1}$$

The modulation frequency (f_w) can thus be defined as the inverse of the cycle period:

$$f_w = \frac{1}{t_{tot}} \tag{2}$$

Another parameter required to define the temporal modulation is the duty cycle δ which defines the ratio between the exposure time and the cycle duration:

$$\delta = \frac{t_{on}}{t_{on} + t_{off}} \tag{3}$$

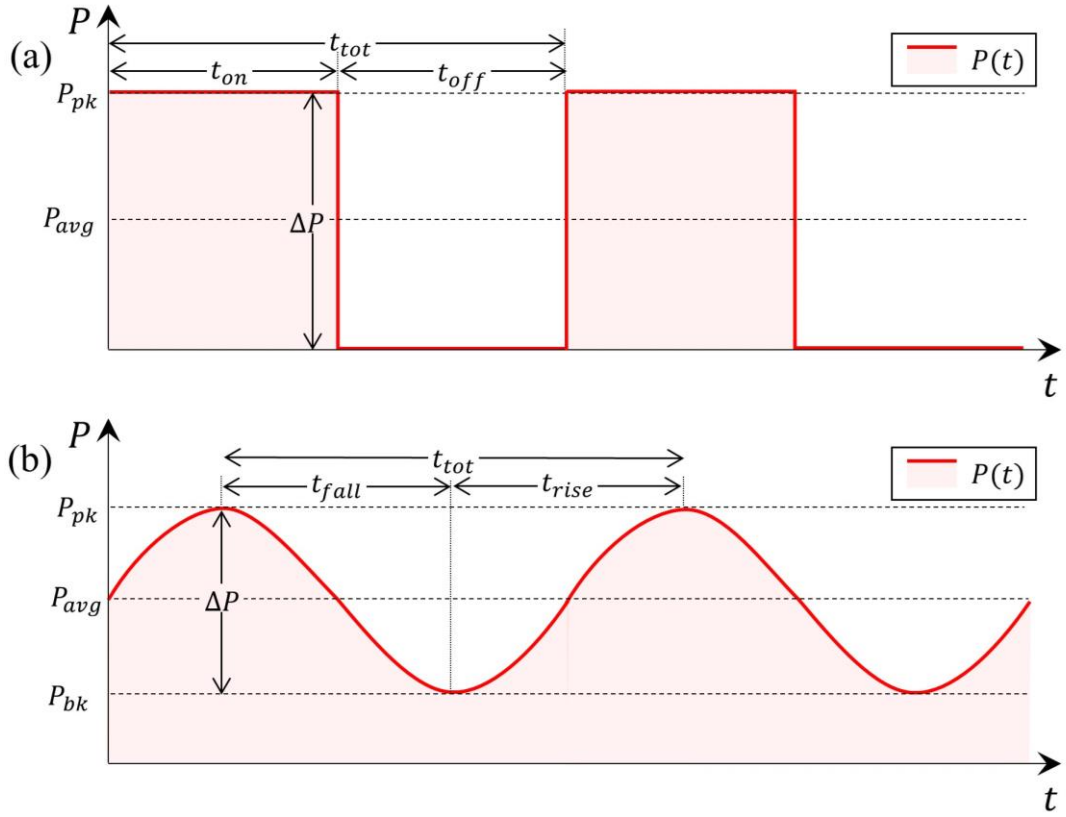

Figure 2. Laser temporal profile parameters for (a) conventional modulation (b) generic modulation waveform

However, in the case of a generic waveform (as in the example of Figure 2 (b)) it is possible to provide a more generalised definition of the pulsation parameters considering also rise and fall times of the modulation waveforms in accordance with the standard ISO 11554 and to previous publications by Temmler *et al.*[34]. We may consider a waveform which oscillates between two non-zero values of the laser emission hence a background emission parameter P_{bk} should be defined to indicate the trough value of the power profile. The amplitude of the waveform ΔP will thus correspond to:

$$\Delta P = P_{pk} - P_{bk} \tag{4}$$

The power emission can thus be viewed as oscillating around an average value P_{avg} of the emission profile which may be defined in its most generic form as:

$$P_{avg} = \frac{1}{t_{tot}} \cdot \int_{t_0}^{t_0+t_{tot}} P(t_i)\ dt \tag{5}$$

where the integral operates over one cycle of the laser emission waveform averaging the power emitted at each time instants $P(t_i)$ starting from a generic time instant t_0. In the case of specific temporal profiles, it is possible to simplify such expression but results are not reported for brevity. A further parametrisation of the emission profile may be obtained by defining the time for the power emission to increase from the trough value to the peak power as rise time t_{rise}. On the other hand, the period between a peak and a trough is defined as the fall time t_{fall} of the laser emission.

Under the hypothesis of a laser beam moving at a constant velocity v, it is also possible to define the distance travelled by the laser beam between two successive peaks, which is also known in literature as the spatial wavelength of the process (λ_w)[35]:

$$\lambda_w = \frac{v}{f_w} \tag{6}$$

2.2 Analytical model to determine recoil pressure variations

The interaction of a continuous wave or temporally modulated laser beam acting upon the surface of the Laser Powder Bed Fusion process may be modelled using a moving point heat source model to estimate the surface temperature of the molten metal. Once the surface temperature of the molten metal is known, it is then possible to estimate the recoil pressure variations according to typical Clausius-Clapeyron relationship[36]. The interaction of a continuous wave or temporally modulated laser beam acting upon the surface of the Laser Powder Bed Fusion process may be modelled using a moving point heat source model to estimate the surface temperature of the molten metal. Once the surface temperature of the molten metal is known, it is then possible to estimate the recoil pressure variations according to typical Clausius-Clapeyron relationship[36]. Other dynamical components (such as capillary or thermo-capillary forces), were not considered in this model due to the fact that they have been reported to be smaller in orders of magnitude and may be considered as secondary effects over the fluid motion[37,38].

The solution to the thermal problem was firstly derived by Carslaw and Jaeger and successively applied by Rosenthal to studies relative to the welding technology[39–41]. Such formulations have been extensively applied to different laser based processes ranging from welding, cutting and heat treatments[42–44]. More recently, such analytical modelling approaches have been employed to study the LPBF process [15,45]. The determination of the temperature distribution allows the understanding of the fundamental mechanisms which regulate a technological process and predicting the effect of process parameter variations. In the present work, an analytical model based on a temporally modulated point heat source was employed as a basis to investigate the changes in terms of melt morphology and induced recoil pressure variations during the single track LPBF deposition process. The model was employed by Simon *et al.* to study heat conduction during deep penetration welding whilst the full derivation of the equations may be found in the book by Dowden[33,46].

In Figure 3, the physical domain modelled is reported, whereby a laser beam interacts at the centre of a relative coordinate system (x,y,z) (moving with the beam at a translational velocity v with respect to the absolute reference system (x',y',z')) and generic temporal power emission profile $P(t)$ defined parametrically according to section 2.1 Laser waveform parameters. A first hypothesis introduced in modelling the deposition process relates to the

material properties which are considered to correspond to the values of the bulk material (thus neglecting the thin powder bed geometry) and their distribution as homogeneous and isotropic. Secondly, the phase transition to liquid is neglected and the point-source solution is considered valid until the material achieves its vaporization temperature.

Such hypothesis clearly introduce approximations to the solution since several studies have shown the significant influence of the geometry and varying thermophysical properties of the powder bed during the LPBF process. For instance, Boley *et al.* and Gusarov reported the variations in beam absorption due to the geometrical nature of powder [47,48]. Thermal conductivity and emissivity are also modified by the powder bed relative density and may for instance be modelled accordingly with the work by Sih and Barrow[49]. Phase transition alongside with varying thermophysical properties at different temperature levels are clearly significant factors in determining the melting and solidification dynamics in the LPBF process. Moreover, the chemical composition of the metallic powder as well as its oxidation state can modifying the consolidation behaviour since they may affect the material emissivity as well as the same process dynamics[50,51].

Nonetheless, in the present model the material was assumed as a bulk solid in order to maintain fixed material properties which enable to solve analytical the mathematical problem formulated. Analogously, constant material properties with respect to temperature were also assumed in order to allow for the mathematical formulation of the solution. On the other hand, it is possible to envision future developments of the present work based on more advanced numerical or semi-analytical approaches which take into account the powder bed geometry and varying thermophysical properties.

A further aspect which is worth mentioning as a possible influential factor on the process outcome is the absorptivity of the material to the laser radiation. This was taken into account by employing a constant multiplicative coefficient of the laser emission power (i.e. which may be considered as the thermal process efficiency). Still, this approach yields some limitations in the model estimate since time-varying absorptivity has been reported in literature and is known to vary with the surface inclination[52]. The analytical solution would require the *a priori* knowledge of such trends or a semi-analytical solution may be calibrated with experimental

data which however go beyond the scope of the present work. Alternatively, more complex approaches, for instance via ray tracing techniques, would require the numerical implementation of the problem. Analogously to the absorptivity, a time-varying emissivity may be expected during the LPBF process. However, in the current formulation of the physical problem with the hypothesis of a purely conductive condition (i.e. no radiative heat transfer) such effects could not be accounted for.

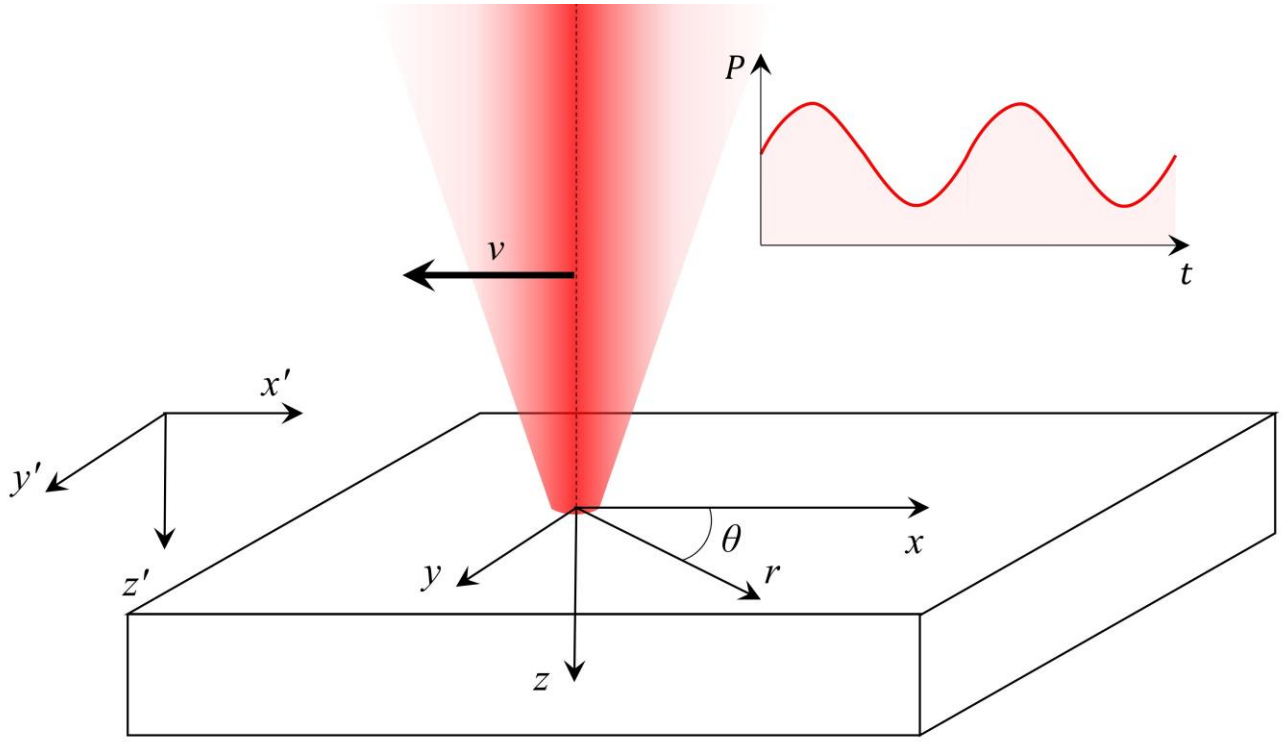

Figure 3. Schematic representation of the point heat source problem with a temporally modulated laser beam

Given such hypothesis and starting from Fourier's heat transfer equation it is possible to derive the point source solution as reported by Dowden [46]. It is possible to formulate the initial equation in terms of the auxiliary solution $S(x,y,z,t)$:

$$T(x,y,z,t) = T_{amb} + S(x,y,z,t) \times \exp\left\{\frac{vx}{2\alpha}\right\} \tag{7}$$

Where α is the thermal diffusivity defined as:

Where k is the thermal conductivity, ρ the material density and c_p the specific heat capacity. The auxiliary solution

$$\alpha = \frac{k}{\rho c_p} \tag{8}$$

$S(x,y,z,t)$ may be searched such that it depends only on the radial distance from the origin r in the case the reference system is positioned on the heat source. The radial distance can be calculated as:

$$r = \sqrt{x^2 + y^2 + z^2} \tag{9}$$

It is then possible to derive the solution of the time-independent temperature field distribution continuous wave emission T_{CW} as follows:

$$T_{CW}(x,r) = T_{amb} + \eta \cdot \frac{P_{avg}}{2\pi kr} \exp\left\{\frac{v}{2\alpha}(x-r)\right\} \tag{10}$$

Where η is the process efficiency coefficient and takes into account losses correlated to the heat transfer mechanisms and material absorptivity, P_{avg} the average power of the continuous wave emission (which will also correspond to the peak emission value in this specific condition). On the other hand, in the case of a temporally modulated problem, by using the separation of variables between space and time, the solution we must look for corresponds to:

$$\phi(x,r,t) = \mathrm{Re}\left\{S(r) \cdot e^{i\omega_w t + \frac{vx}{2\alpha}}\right\} \tag{11}$$

Where ϕ is the new solution that must be sought for starting from the previous auxiliary solution *S(r)* (see Dowden for details regarding the mathematical derivation [53]). The waveform frequency effect is reported by the imaginary vector rotating at angular frequency ω_w which may be defined as:Where ϕ is the new solution that must be sought for starting from the previous auxiliary solution *S(r)* (see Dowden for details regarding the mathematical derivation [53]). The waveform frequency effect is reported by the imaginary vector rotating at angular frequency ω_w which may be defined as:

In order to achieve the final solution, the same approach employed for the CW emission case may be applied

$$\omega_w = 2\pi f_w \tag{12}$$

(following the derivation by Dowden)[46]. For compactness of the formulation, we may define Simon's number which indicates the relationship between the translation speed of the heat source *v* and the velocity of propagation of the thermal partial waves $\sqrt{4\alpha\omega_w n}$ [33]:

$$\mathrm{Si} = \frac{8\pi f_w \alpha}{v^2} \tag{13}$$

Under the hypothesis of linearity, imposing that the solution must be real and considering that the power input may be expressed through a Fourier series, it is possible to express the time-dependent temperature solution as:

$$\begin{aligned} T(x,r,t) = T_{CW}(x,r,t) &+ \frac{1}{2\pi\kappa r}\sum_{n=1}^{+\infty} a_n \times \mathrm{Re}\left(\exp\left\{2\pi f_w n t\cdot i + \frac{v}{2\alpha}\left(x - r\sqrt{1+n\cdot \mathrm{Si}\cdot i}\right)\right\}\right) \\ &+ \frac{1}{2\pi\kappa r}\sum_{n=1}^{+\infty} b_n \times \mathrm{Re}\left(\exp\left\{2\pi f_w n t\cdot i + \frac{v}{2\alpha}\left(x - r\sqrt{1+n\cdot \mathrm{Si}\cdot i}\right)\right\}\right) \end{aligned} \tag{14}$$

Where a_n and b_n are the coefficients of the Fourier series for the different power input waveforms and are reported in Table 1.

Table 1. Coefficients of the Fourier series for the different waveforms

Waveform	a_n	b_n
Square Wave	$\frac{2\Delta P}{n\pi}\sin(n\pi t_{on}\cdot f_w)$	$-$
Triangle Wave	$\frac{4\Delta P}{n^2\pi^2}\sin^2\left(\frac{n\pi}{2}\right)$	$-$
Ramp Up Wave	$-$	$-\frac{\Delta P}{n\pi}(-1)^n$

Waveform	a_n	b_n
Ramp Down Wave	$-$	$=\frac{\Delta P}{n\pi}(-1)^n$

Once the surface temperature of the liquid mass is estimated using the point heat source model, it is thus possible to estimate the recoil pressure induced on the molten material as indicated in literature. The relationship between surface temperature and recoil pressure was first formulated by Anisimov in 1968[54]. The more commonly accepted relationship to model the relation between the recoil pressure p_r and surface temperature T_s relates to the Clausius-Clapeyron equation[36]:Once the surface temperature of the liquid mass is estimated using the point heat source model, it is thus possible to estimate the recoil pressure induced on the molten material as indicated in literature. The relationship between surface temperature and recoil pressure was first formulated by Anisimov in 1968[54]. The more commonly accepted relationship to model the relation between the recoil pressure p_r and surface temperature T_s relates to the Clausius-Clapeyron equation[36]:

$$p_r = \frac{(1+\beta_r)}{2} \cdot p_0 \cdot e^{\frac{\Delta H_v}{k_b}\left(\frac{1}{T_{vap}}-\frac{1}{T_s}\right)} \tag{15}$$

Where β_r is the recondensation factor, ΔH_v is the enthalpy of phase transition, T_{vap} the vaporisation temperature, k_b is Boltzmann's constant, p_0 the ambient pressure. The coefficient β_r is considered as 0.18 under high evaporation conditions (according to calculations by Knight)[55]. the enthalpy of phase transition may be calculated as follows[36]: Where β_r is the recondensation factor, ΔH_v is the enthalpy of phase transition, T_{vap} the vaporisation temperature, k_b is Boltzmann's constant, p_0 the ambient pressure. The coefficient β_r is considered as 0.18 under high evaporation conditions (according to calculations by Knight)[55]. the enthalpy of phase transition may be calculated as follows[36]:

where m is the mass per atom and L_v is the latent heat of vaporization.

$$\Delta H_v = m \cdot L_v \tag{16}$$

3 Recoil pressure variation in LPBF with variable laser emission waveforms

3.1 Modelled LPBF conditions

The aim of the present work is to provide an preliminary investigation regarding the effect of different temporal waveforms during the LPBF process. Hence, the simulation campaign was designed to explore the impact of different temporal emission profiles on the melt motion by comparing the high speed videos with the predictions of the recoil pressure estimation model. The modelled conditions were designed to provide a constant energy per scan track. Hence, the laser scanning speed (v) was fixed at 300 mm/s and the average emission power (P_{avg}) at 200W. Such conditions in the case of continuous wave emission of the laser power (i.e. without temporal modulation) were shown to provide a stable process for the realisation of thin walled specimens and which thus was kept as reference condition. Four different wave shapes were investigated, namely Square Wave (SQW), Triangle Wave (TRW), Ramp Up Wave (RUW) and Ramp Down Wave (RDW). Square Wave with a duty cycle level of 50% was considered representative of typical processing conditions when employing modulated emission as investigated in past research by the Caprio *et al.* [15]. On the other hand, the other waveforms exhibited shapes with gradual increases in laser emission power from the background to the peak level (corresponding to Ramp Up), gradual decreases (Ramp Down) and both a gradual increase and decrease (i.e. Triangle Wave emission). In Figure 4, their schematic representation is reported.

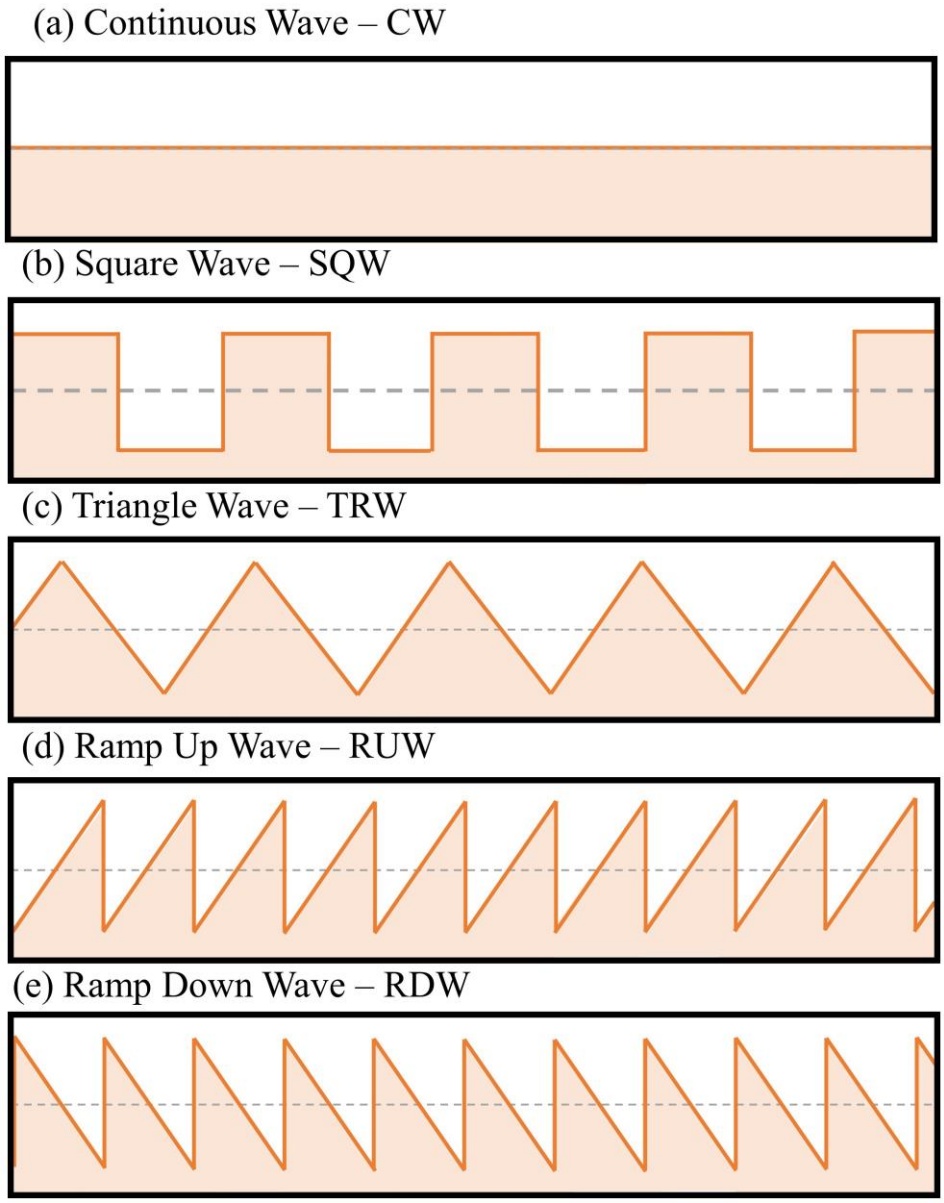

Figure 4. Different waveform shapes tested (a) reference case Continuous Wave *CW* (b) Square Wave *SQW* (c) Triangle Wave *TRW* (d) Ramp Up Wave *RUW* (e) Ramp Down Wave *RDW*

Four different levels of wave frequency were associated to the present investigation (f_w=2-4-6-8 kHz) such that the spatial wavelength of the waveform did not exceed twice the waist diameter of the laser beam (λ_w correspondingly ranging from 150 to 36 µm). Two levels of amplitude ΔP were associated to the waveforms such that power oscillated between P_{bk}=100 and P_{pk}=300 W and between P_{bk}=0 and P_{pk}=400 W (i.e. ΔP=200-400 W). AISI 316L stainless steel was chosen as an established material for LPBF processability. Linear paths of 20 mm

length with associated the different experimental conditions were simulated over a 50 µm thick powder bed. The details of the experimental campaign are reported in Table 2.

Table 2. Fixed and variable factors of experimental campaign

Fixed factors	
Material	AISI316L
Average power, P_{avg} (W)	200
Scan speed, v_s (mm/s)	300
Layer thickness, l_t (µm)	50
Variable factors	
Temporal waveforms	Square Wave – Triangle Wave Ramp Up – Ramp Down
Wave frequency, f_w (kHz)	2 – 4 – 6 – 8
Wave Amplitude, ΔP (W)	200 – 400

3.2 Implementation of the analytical model to estimate recoil pressure variations

The analytical model to estimate the recoil pressure variations was implemented in Matlab. The thermophysical properties of AISI316L used in the analytical model of the present work were taken from Mills [56] and Kim [57] and are reported in Table 3. The value of the latent heat of vaporisation L_v of iron was taken from literature and was used to approximate the value of AISI 316L since Fe is the main alloying element [58,59]. The process efficiency coefficient η of the model was calibrated using the simulations of the continuous wave emission and using preliminary experimental data. The parameter η was regulated in a way such that the melting iso-therm corresponded to the measured track width, according to the methodology presented in a previous work[15].

Table 3. Thermophysical properties of stainless steel AISI316L at liquidus temperature [56,57] **and other significant parameters of the analytical model. Asterisk indicates properties for Fe which were considered in absence of values for AISI316L**[58,59]**. Thermophysical properties of stainless steel AISI316L at liquidus temperature** [56,57] **and other significant parameters of the analytical model. Asterisk indicates properties for Fe which were considered in absence of values for AISI316L.**

Property	**Value**
Specific heat capacity, c_p (J/kg·K)	830
Density, ρ (kg/m^3)	6881
Thermal conductivity, k (W/m·K)	27
Thermal diffusivity, α (m^2/s)	$4.73 \cdot 10^{-5}$
Solidus temperature, $T_{solidus}$ (K)	1658
Liquidus temperature, $T_{liquidus}$ (K)	1733
Vaporisation temperature, T_{vap} (K)	3090
Latent heat of vaporization*, L_v (J/kg)	$6.088 \cdot 10^6$

Mass per atom, m (kg)	$9.27 \cdot 10^{-26}$
Process efficiency, η	0.13
Boltzmann's constant, k_b (J/K)	$1.380649 \cdot 10^{-23}$

The numerical solution of the thermal model requires a limited value for the order of the Fourier transforms. In order to minimise the error introduced with such approximations, a set of preliminary simulations were conducted to evaluate the influence of such parameter. The order of the transforms was set to n=100 which does not introduce significant approximations from a numerical perspective. The simulation domain was varied between -50 and 400 µm along the x-coordinate and between -150 µm and 150 µm along the y-coordinate whilst it was evaluated at the top surface of the laser-material interaction corresponding to a 0 µm z-coordinate. With regards to the temporal domain, the mathematical model was evaluated on a 1500 µs range (which corresponded to a minimum of three waveform periods at the lowest waveform frequency) with a 10 µs resolution. The information related to the simulation domain are summarized in Table 4.

Table 4. Spatial and temporal domains of the simulation with their resolution

Domain		Range	Resolution
Spatial	x	[-50 µm; 400 µm]	1 µm
	y	[-150 µm; 150 µm]	1 µm
	z	0 µm	-
Temporal	t	[0 µs; 1500 µs]	10 µs

4 Results

4.1 Temperature field and recoil pressure

4.1.1 Effect of different waveforms

In order to view the effects of the different waveforms from a temporal perspective, the time-varying history of a point behind the origin of the coordinate system (where the modelled laser material interaction occurs) was selected, with coordinates which correspond to x=50 µm, y=5 µm and z=0µm. However, this observation point could be moved towards different positions throughout the simulated domain and is taken as a representative reference coordinate. In Figure 5, the temporal variations of the temperature and pressure profiles at this specific coordinate point are reported for the conditions simulated with a waveform amplitude ΔP=200W and waveform frequency f_w=2 kHz. Accordingly with the mathematical model developed, the peak recoil pressure values shown in Figure 5 occur in correspondence with the peak temperature values and indicate a periodical behaviour. The pressure and temperature peaks are slightly shifted in the temporal domain with respect to the power input and this can be correlated to the time period the temperature wave induced by the temporally modulated power input takes to reach the coordinates of the simulated position.

As shown in the different cases of Figure 5, the waveforms which possess strong discontinuities in the temporal domain (square wave, ramp up and ramp down), induce instantaneous peaks of greater value in terms of temperature and consequently recoil pressure. These effects are induced by the Fourier series of the waveforms modelled whereas the triangular waveform, which better approximates a sinusoidal shape, reports smoother variations in terms of the recoil pressure induced. In general, strong discontinuities in terms of recoil pressure may generate disturbances on the melt flow. Depending on the application case, such effects may be beneficial rather or detrimental. As shown by Ly *et al.*, resonance excitation of capillary waves may be beneficial during a laser drilling process whereas the same approach would have negative effects during a deposition process if not appropriately controlled [60].

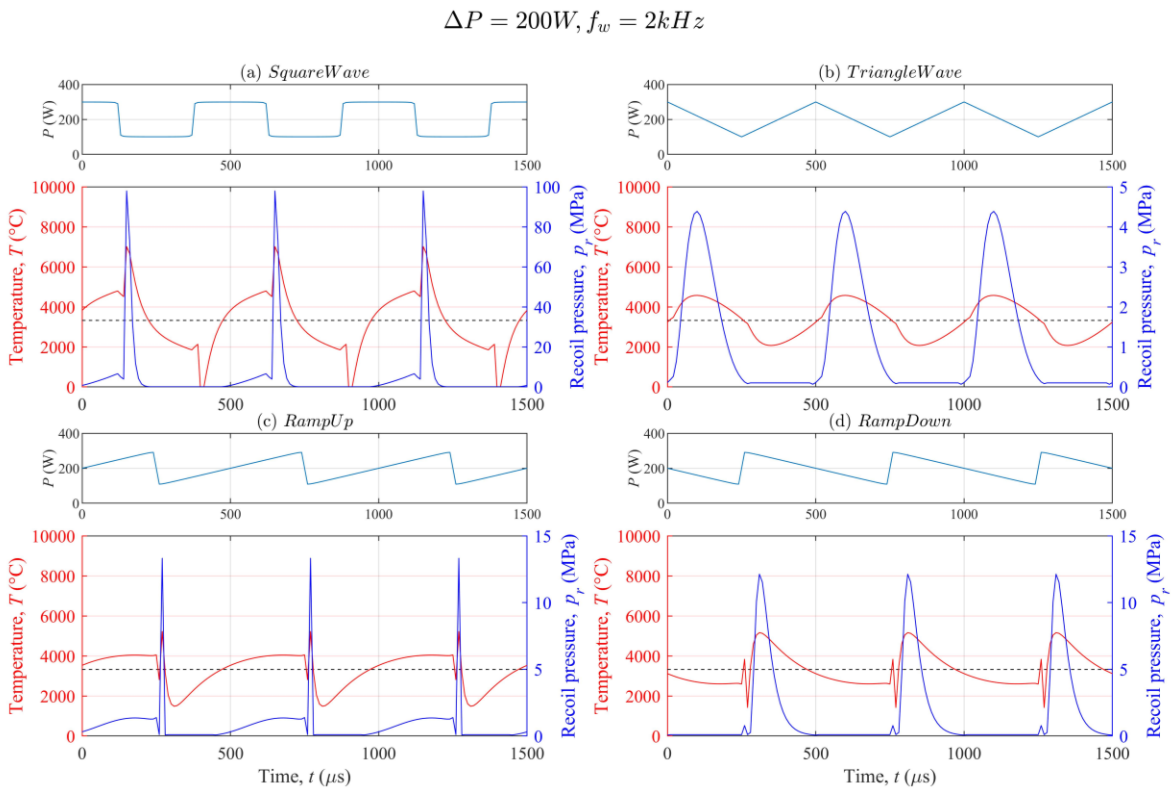

Figure 5. Estimated temperature and pressure at different time instants at a specific position on the melt surface behind the laser material interaction corresponding to *x*=50 µm, y=5 µm, z= 0 µm for the different waveforms (a) Square, (b) Triangle, (c) Ramp Up and (d) Ramp Down with ΔP=200 W and f_w=2kHz. Dashed black line represents reference temperature estimated with CW emission.

In order to assess, if there is a correspondence between the input waveform and the recoil pressure induced on the melt flow it is possible to estimate the Power Spectral Density (PSD). Figure 6 reports the PSD estimate for the different waveforms with ΔP=200W and f_w=2 kHz. The correspondence between the fundamental frequency of the input power waveform and its higher order components is clearly visible. Hence, the recoil pressure induced by the temporal power variations will be acting as a periodical forcing input on the surface of the melt pool. It must be noted that fast variations in terms of power input tend to generate the peaks with greater magnitude in terms of recoil pressure (as visible in Figure 5, in the case of the Square waveform with respect to the other waveforms).

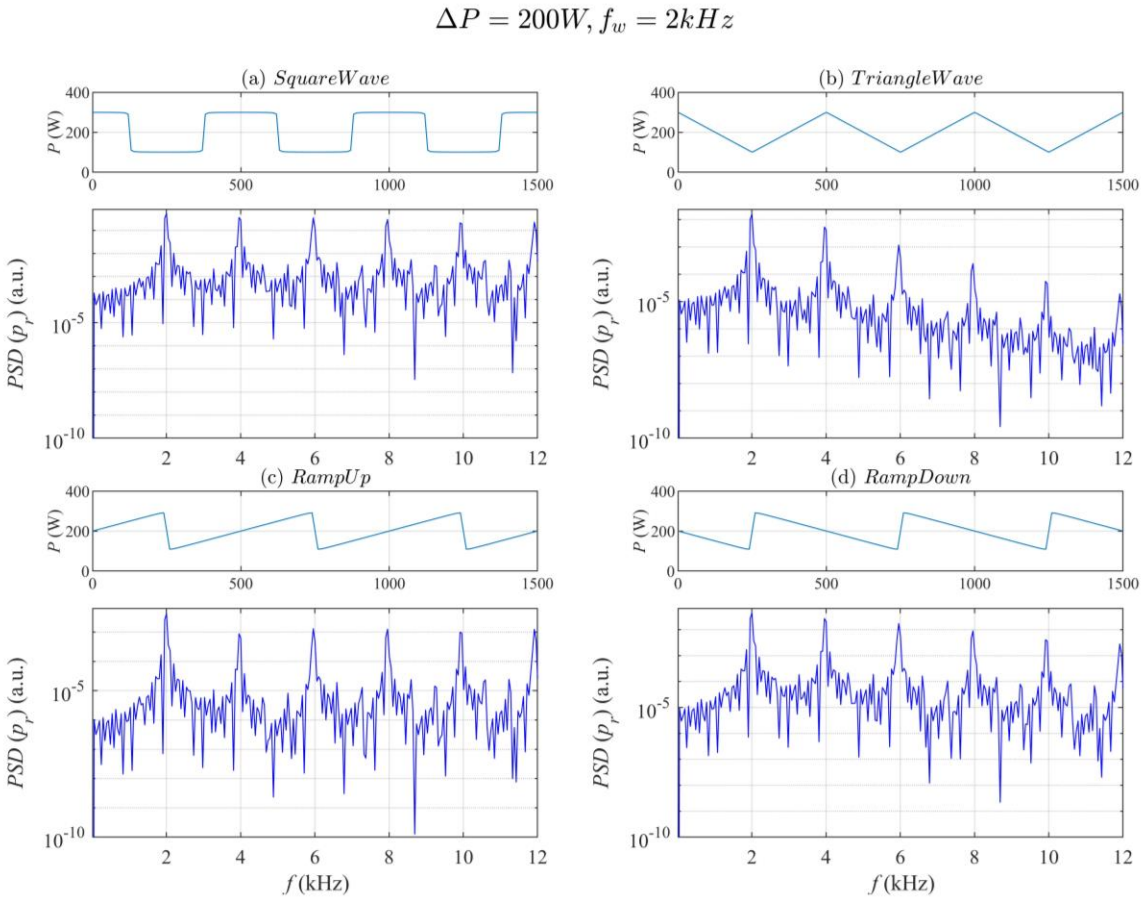

Figure 6. Power Spectral Density estimate of the recoil pressure p_r simulated with the analytical model for different waveforms at a specific position on the melt surface behind the laser material interaction corresponding to *x*=50 µm, y=5 µm, z= 0 µm

The temperature distribution on the surface of the material when the different waveforms are employed may be observed at a specific time instant in Figure 7 and at different time instants in supplementary video n°1. The mathematical model developed shows the propagation of thermal waves throughout the material. The propagation behaviour of the heat input, as previously indicated, is strongly correlated to the recoil pressure variations. The triangular waveform, which does not exhibit sudden variations in terms of power input (due to ramping up and down effect between peaks) shows a gradual propagation of the heat waves, whereas the other waveforms appear to be symptomatic of greater instabilities in the presence of discontinuities.

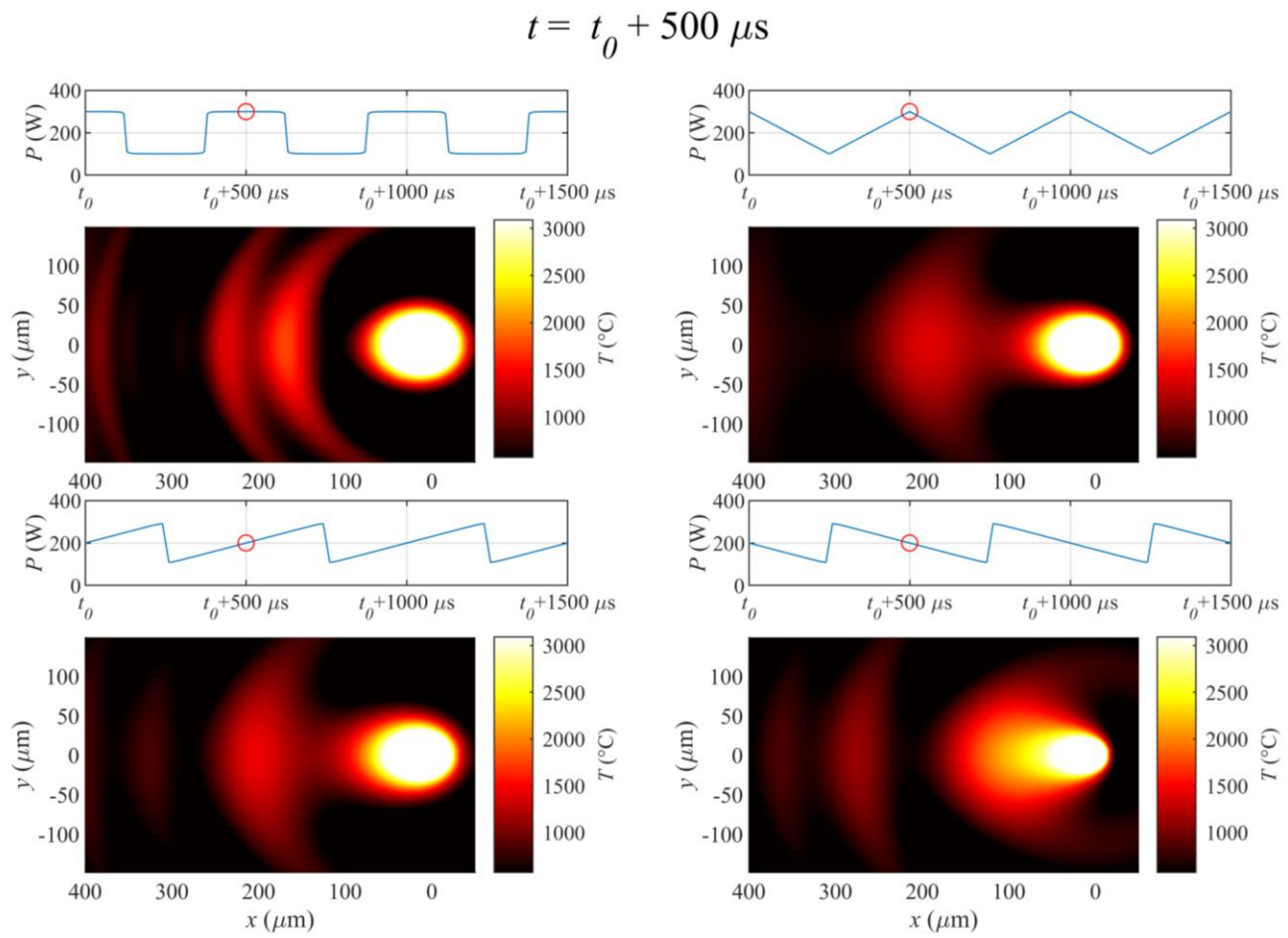

Figure 7. Temperature distribution in the x-y field at a time instant of the simulation corresponding to $t=t_0$+500 μs for the different waveform shapes with ΔP=200W, f_w=2 kHz. The reader is referred also to supplementary video n°2 which reports the recoil pressure variations at the different time instants. The colour scaling of temperature is limited at the vaporisation temperature of AISI316L to improve visualization of the temperature waves induced by the time-varying power input.

Figure 8 reports the temperature and recoil pressure variations of a specific coordinate when waveforms with a greater amplitude are employed (ΔP=400W). Interestingly enough, the Square Wave emission condition simulated is representative of modulated emission typically employed during the LPBF process with fiber laser sources (i.e. when the power emission varies between 0 W and the peak emission level)[8]. Once again, it is possible to denote that in such operative condition, recoil pressure variations will achieve the highest magnitude symptomatic of process instabilities which may be induced in the melt flow. Ramping up and down of the power input allows to avoid significant variations in the recoil pressure. As reported in Figure 8 (c) for the Ramp Up waveform, the peak in recoil pressure occurs when there is a sudden decrease in power. This phenomenon is known to generate defects according to previous work by Khairallah *et al.* due to the sudden collapse of the vapour depression generated by

the high intensity laser beam and is captured mathematically in the results of the analytical model hereby proposed [30]. The ramp down profile, analogously impinges on the melt flow dynamics of the process, by introducing a rapid increase in terms of recoil pressure which can generate significant disturbances on the melt flow. Contrarily to the Ramp Up mechanisms, the period of time where an elevated recoil pressure acts on the surface of the material is increased and this might be considered as a further detrimental aspect.

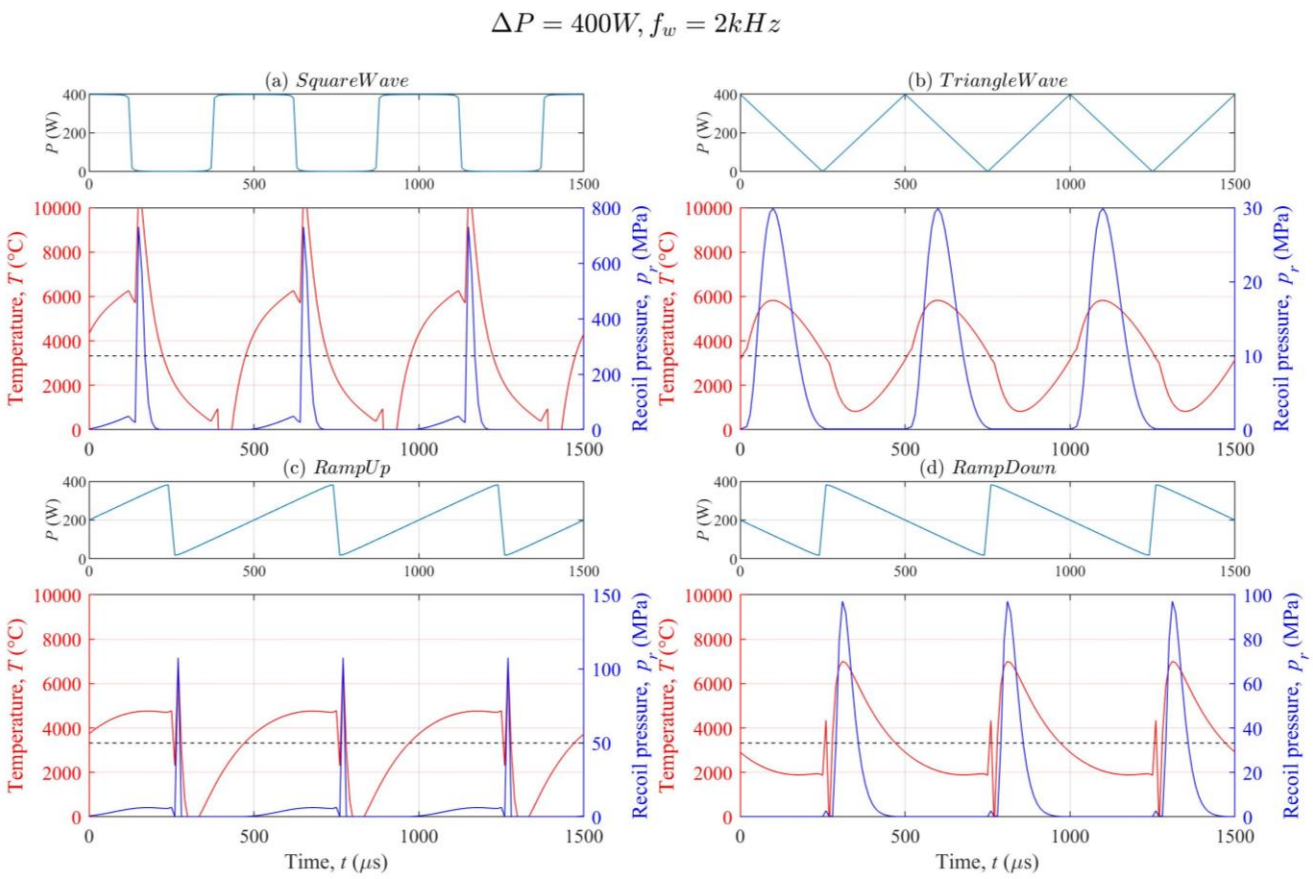

Figure 8. Estimated melt surface temperature and recoil pressure at different time instants at a specific position on the melt surface behind the laser material interaction corresponding to *x*=50 µm, y=5 µm, z= 0 µm for the different waveforms (a) Square, (b) Triangle, (c) Ramp Up and (d) Ramp Down with ΔP=400 W and f_w=2kHz. Dashed black line represents reference temperature estimated with CW emission.

In order to observe the extent of the region whereby the recoil pressure acts over the melt region, it is possible observe Supplementary video n°2, which reports the extension of the recoil pressure interaction region by limiting numerically the value at p_r= 10 MPa. The effect of the heat waves generated by the fast power variations when rapidly ascending power profiles are employed is visible from a spatial perspective. As anticipated by the recoil

pressure trends reported in Figure 5 and Figure 8, the peaks in recoil pressure are translated in interaction waves which act throughout the surface of the liquid and may eventually induce variations in the liquid motion.

Recoil pressure levels have been simulated by Kouraytem *et al.* in the order of 1 MPa and found to be orders of magnitude greater than the capillary and thermocapillary forces (respectively with values of 10^4 Pa and 10^3 Pa)[38]. Experimental measurements by Cullom *et al.* reported values for the recoil pressure in the range of tens of kPa which were found to be in agreement with the results reported by Yin *et al.*[37,61]. Although, the recoil pressure levels reported in the current work are well beyond values reported in literature they still confirm the predominance of the recoil pressure over other dynamic components. This is correlated to the analytical nature of the model, typical of moving point heat source models, which estimates infinite surface temperatures in the origin of the relative reference system. This obviously impinges on the estimate of the recoil pressure. Nonetheless, when moving outwards radially from the origin the numerical value returns within expectable values and may be found coherent with the nature of the physical problem under analysis. Even though the recoil pressure values estimated within this work should be considered as rough estimates, considering the predominance of the recoil pressure over other dynamic components, the periodical forcing input induced over the melt pool by the time varying power emission is a phenomenon expected to occur (as predicted in the PSD of Figure 6).

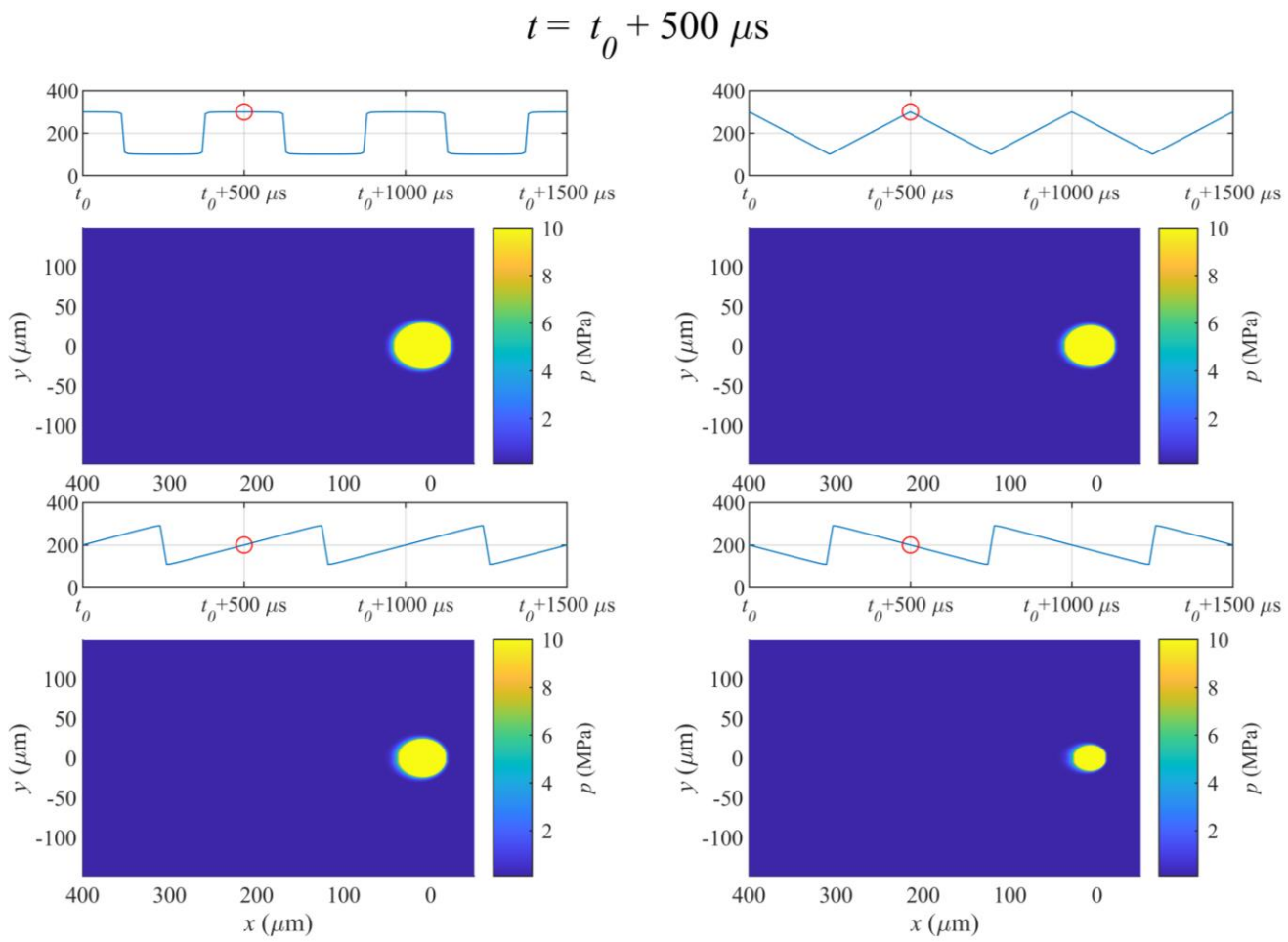

Figure 9. Pressure distribution in the x-y field at a time instant of the simulation corresponding to $t=t_0+500$ µs for the different waveform shapes with ΔP=200W, f_w=2 kHz. The reader is referred also to supplementary video n°2 which reports the recoil pressure variations at the different time instants. The colour scaling of the pressure is limited at 10 MPa to enhance the visualisation.

4.1.2 Effect of waveform amplitude and frequency

A further aspect to be considered when defining the laser waveform parameters to be employed during the LPBF fabrication process, is the possibility of regulating the waveform frequency f_w alongside the waveform amplitude. Figure 10 reports the effect of different waveform frequencies at two levels of amplitude for the Square Wave. As anticipated, higher levels of peak power emission generate higher surface temperatures on the melt which eventually induce greater oscillations in terms of recoil pressure.

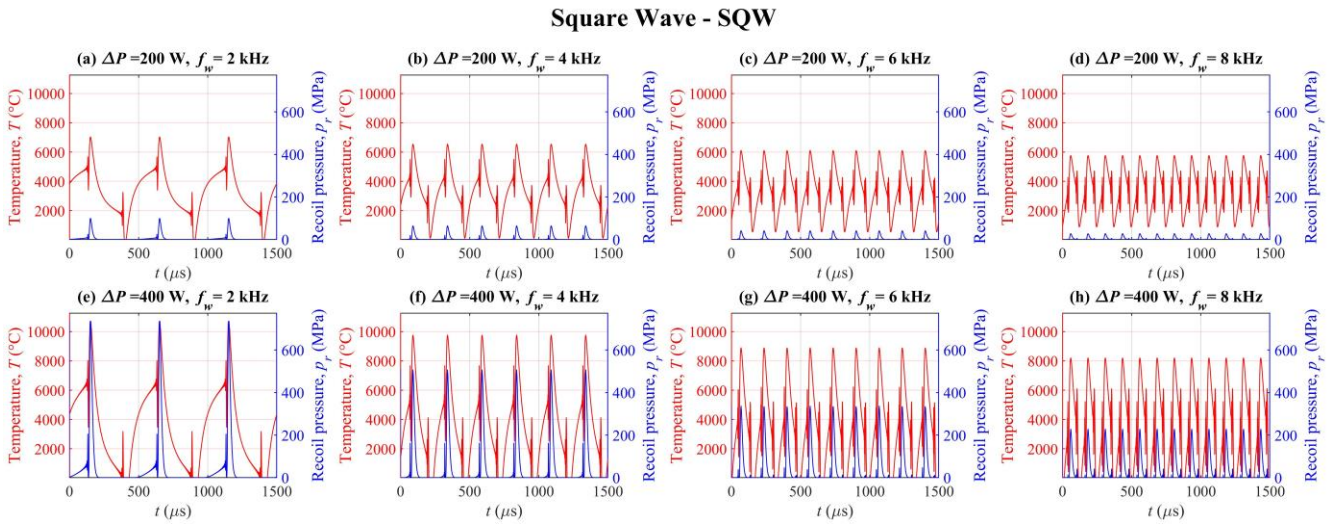

Figure 10. Estimated melt surface temperature and recoil pressure at different time instants at a specific position on the melt surface behind the laser material interaction corresponding to *x*=50 μm, y=5 μm, z= 0 μm for different levels of waveform amplitude (ΔP=200 W for (a)-(d), ΔP=400 W for (e)-(h)), and waveform frequency for Square Wave.

The effect of power modulation at different levels of f_w and ΔP when a triangular waveform is employed is reported in Figure 11. The temperature variation exhibits a quasi-sinusoidal oscillation without strong discontinuities. This effect could be expected since the triangular waveform best approximates a sinusoidal variation and is in accordance with Fourier's transform employed to mathematically solve the heat conduction problem. The gradual increase in temperature implies that the recoil pressure variations occur more gently with respect to the other waveform shapes, as previously shown in Figure 5 and Figure 8, and confirmed at different levels of waveform frequency in Figure 11. As the waveform frequency increases it is possible to view that the estimated temperature profile responds accordingly, tending towards the formation of discontinuities in the temperature oscillations induced. When such event occurs at f_w=8 kHz for the Triangle Wave (Figure 11 (d) and (h)), the peak recoil pressure increases and may be symptomatic of instabilities. On the other hand, the peak recoil pressure decreases monotonically for increasing values of waveform frequency in the case of Square wave emission (as visible in Figure 10).

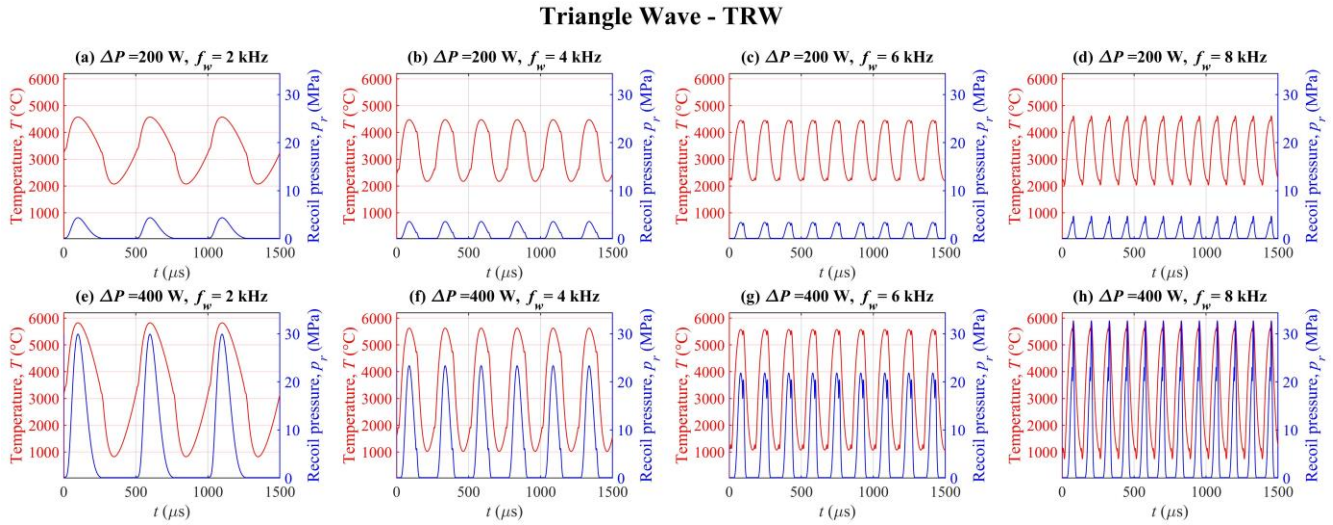

Figure 11. Estimated melt surface temperature and recoil pressure at different time instants at a specific position on the melt surface behind the laser material interaction corresponding to *x*=50 μm, y=5 μm, z= 0 μm for different levels of waveform amplitude (ΔP=200 W for (a)-(d), ΔP=200 W for (e)-(h)), and waveform frequency for Triangle Wave.

Figure 12 reports the Power Spectral Density estimate of the recoil pressure applied on the representative position x=50 μm, y=5 μm, z= 0 μm for the Square Wave and Triangle Wave. As anticipated in Figure 6, the waveform frequency corresponds to the measured. If we may consider a linear mechanical system, then we can expect that the liquid will oscillate at the same frequency ($f_{osc,theo}$) as the imposed waveform frequency. It is thus possible to formulate the following relationship independently of the waveform shapes and amplitude.

$$f_{osc,theo} = f_w \tag{17}$$

Different levels of waveform amplitude, as shown by the time-varying signals of the recoil pressure (Figure 10 and Figure 11). This difference is expected to have an effect also on the oscillatory behaviour of the melt as confirmed by the PSD estimates of the signal reported in Figure 12 which show remarkably lower peaks in terms of amplitude of the PSD spectrum in the case of ΔP=200W. Hence, a modification of the waveform amplitude can be expected to have a significant effect over the melt dynamics. Excessive levels of amplitude may generate instabilities and melt ejections, whereas smaller variations may not significantly affect the melt motion if we considering that viscous forces with a dissipative effect will be effectively be present.

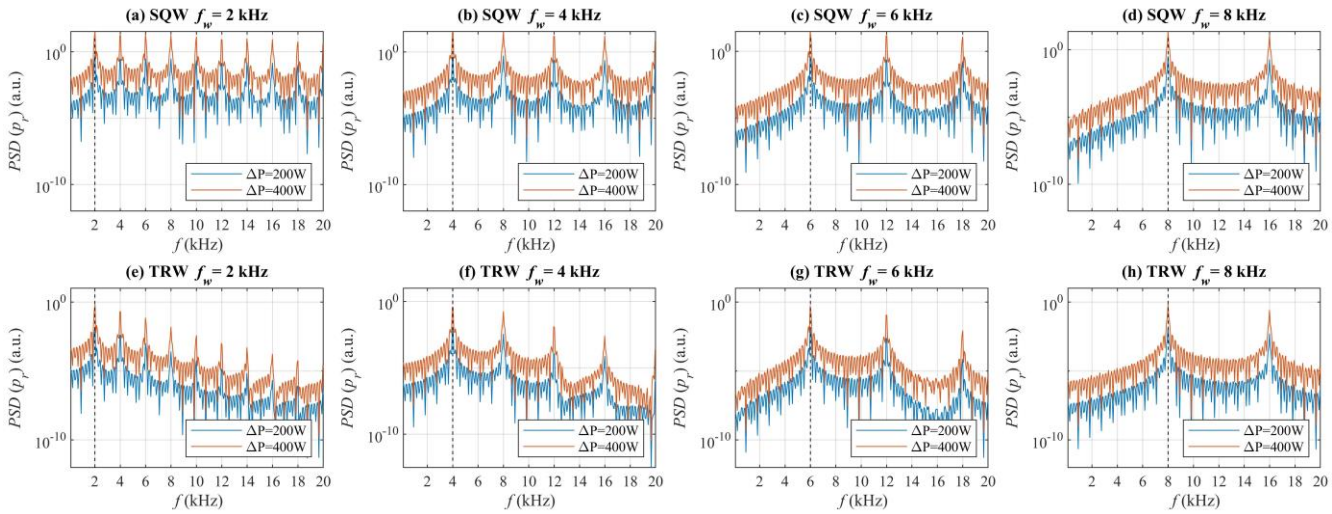

Figure 12. Power Spectral Density estimate of the estimated recoil pressure at position *x*=50 µm, y=5 µm, z= 0 µm. Orange and blue indicate waveform amplitude level of ΔP=200 W and ΔP=400 W. Dashed black line indicates nominal waveform frequency f_w. Waveform shape indicated in the graph title.

5 Discussion

The variation of the maximum temperature estimated in a specific position with the different pulsation mechanisms and their parameters is reported in Figure 13. This graph may be read also considering the exact correspondence between the imposed waveform frequency f_w and the theoretical frequency of oscillation of the melt induced f_{osc} that could be disclosed via the PSD estimates. As formulated in the analytical model, the recoil pressure generated over the melt flow is correlated to the surface temperature through the exponential equation of the Clausius-Clapeyron relation. It is interesting to view that the maximum temperature is correlated to the waveform frequency imposed thus indicating a strong interplay between the different parameters. Discussion of such effects and relations is correlated to Simon's number introduced in the publication by Simon *et al.* and by Dowden[33,53]. The current work expands the previous results showing the effect of different waveform shapes under typical conditions retrievable in the LPBF process. The effect of pulsation frequency was experimentally observed by Morgan *et al.* showing that higher frequencies increased the densification of metal powders in the LPBF process [14]. Such behaviour may be considered consistent with the results predicted hereby where an increase in frequency tends to decrease the peak temperatures thus the instabilities that may be induced over the melt pool especially in the case of the most commonly employed waveform.

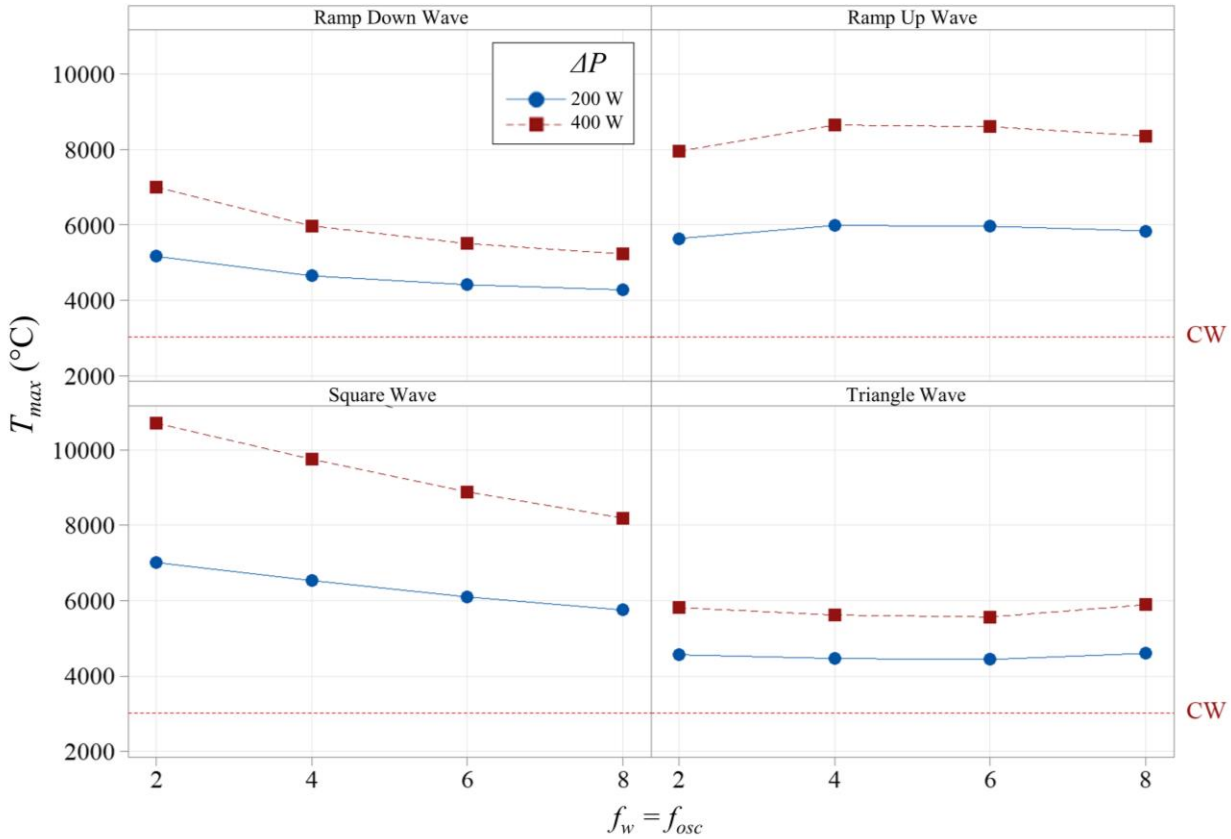

Figure 13. Maximum temperature achieved in the different conditions simulated at the position *x*=50 µm, y=5 µm, z= 0 µm. Reference temperature from simulation of CW emission in dashed red line.

In general, due the higher peak powers considered with respect to the continuous wave emission condition, temporally modulated emission induces higher peak temperatures over the melt consequently generating higher peaks in terms of recoil pressure. On the other hand, it must be considered that a constant process efficiency coefficient was implemented throughout the different conditions simulated. Taking into consideration that the coupling mechanisms between the input laser beam and the molten material are subject to a wide variety of factors, it might be argued that a calibration of the model for the specific waveforms or conditions may appropriate. For instance, such aspects correlated to model calibration have been investigated by Caprio *et al.* in a previous work always dealing with the analytical modelling of the effects of modulated emission[15]. On the other hand, a variation in terms of magnitude of the maximum temperatures achievable at a constant level of process efficiency may provide indications with regards to the amplitude of the oscillatory motion induced (as well as other parameters associated to temperature field generated such as temperature gradients and cooling rates). Still, it must be considered that analytical models based on the point-heat source solution have the intrinsic issue of estimating

temperatures tending towards infinity as the radius of the solution tends to the origin[39]. Advanced computational fluid dynamic modelling may allow to obtain more consistent estimates of the temperature fields which however go beyond of the present work which aimed at providing a fast computational approach to evaluate the principal effects of temporally modulated beams over the melt flow. Still, the combined effect of the different dynamical components acting over the molten liquid (i.e. capillary and thermo-capillary forces), may yield significant effects over the metallurgical properties of the material. In order to obtain more accurate predictions regarding such aspects, as previously mentioned, a numerical thermo-fluid dynamic model may be more effective and will be the attention of future works.

In order to support the theoretical results presented in the current work, Part II of the investigation reports the results from an experimental campaign aimed at replicating the conditions modelled in the present work. The empirical approach intends to validate the analytical model hereby proposed and assess the feasibility of employing temporal beam shaping approaches as a further tool to enhance the LPBF process.

6 Conclusions

The present work provides a stable analytical framework for the estimation of the principal effects in terms of temperature distribution and consequent recoil pressure variations when different waveform parameters are employed during the Laser Powder Bed Fusion process. The model was implemented in conditions considered representative of the LPBF process and temperature and recoil pressure distributions could be estimated.

Triangular waveform emission of the laser power avoids the presence of strong discontinuities in the induced recoil pressure fields over the melt surface. Such effects may be beneficial in controlling the melt flow at a specific frequency. The peak values of recoil pressure during the process were obtained using Square Wave indicating that such waveforms may generate significant disturbances in the melt flow, hence making it more apt for a material removal process rather than a controlled deposition process. Higher waveform form frequencies are beneficial in reducing peak recoil pressure induced on the melt pool unless discontinuities are introduced in the temperature profile.

Greater waveform amplitude induce higher surface temperatures, thus higher oscillations in terms of recoil pressure may create significant disturbances over molten metal, possibly generating instabilities.

In terms of process design, the main indications which may be extrapolated are that waveform modulation may be employed to modify the melt flow frequency unless self-sustained oscillations are desired (which occur in the CW emission regime). Power variations between non-zero values should be employed to avoid excessive disturbances over the melt flow which might cause melt ejections or instabilities.

The future developments of the work deal with the experimental validation of the modelling framework hereby reported.

Acknowledgements

The Italian Ministry of Education, University and Research is acknowledged for the support provided through the Project "Department of Excellence LIS4.0 - Lightweight and Smart Structures for Industry 4.0”.

References

[1] S. Edson, A. F, K. Y, K. Osakada, M. Shiomi, Mechanical properties of pure titanium models processed by selective laser melting, Proc. Solid Free. Fabr. Symp. Solid. 1 (2002) 180–186. https://doi.org/10.1017/CBO9781107415324.004.

[2] C.Y. Yap, C.K. Chua, Z.L. Dong, Z.H. Liu, D.Q. Zhang, L.E. Loh, S.L. Sing, Review of selective laser melting: Materials and applications, Appl. Phys. Rev. 2 (2015) 041101. https://doi.org/10.1063/1.4935926.

[3] T. Ghidini, Materials for space exploration and settlement, Nat. Mater. 17 (2018) 846–850. https://doi.org/10.1038/s41563-018-0184-4.

[4] M. Attaran, The rise of 3-D printing: The advantages of additive manufacturing over traditional manufacturing, Bus. Horiz. 60 (2017) 677–688. https://doi.org/10.1016/j.bushor.2017.05.011.

[5] T. Pereira, J. V. Kennedy, J. Potgieter, A comparison of traditional manufacturing vs additive manufacturing, the best method for the job, Procedia Manuf. 30 (2019) 11–18. https://doi.org/10.1016/j.promfg.2019.02.003.

[6] A. V. Gusarov, S.N. Grigoriev, M.A. Volosova, Y.A. Melnik, A. Laskin, D. V. Kotoban, A.A. Okunkova, On productivity of laser additive manufacturing, J. Mater. Process. Technol. 261 (2018) 213–232. https://doi.org/10.1016/j.jmatprotec.2018.05.033.

[7] J. Grünewald, F. Gehringer, M. Schmöller, K. Wudy, Influence of Ring-Shaped Beam Profiles on Process Stability and Productivity in Laser-Based Powder Bed Fusion of AISI 316L, (2021) 1–18.

[8] L. Caprio, A.G. Demir, B. Previtali, Comparative study between CW and PW emissions in selective laser melting, J. Laser Appl. 30 (2018) 32305. https://doi.org/10.2351/1.5040631.

[9] A.G. Demir, P. Colombo, B. Previtali, From pulsed to continuous wave emission in SLM with contemporary fiber laser sources: effect of temporal and spatial pulse overlap in part quality, Int. J. Adv. Manuf. Technol. 91 (2017) 2701–2714. https://doi.org/10.1007/s00170-016-9948-7.

[10] K. Mumtaz, N. Hopkinson, Top surface and side roughness of Inconel 625 parts processed using selective laser melting, Rapid Prototyp. J. 15 (2009) 96–103. https://doi.org/10.1108/13552540910943397.

[11] K.A. Mumtaz, N. Hopkinson, Selective Laser Melting of thin wall parts using pulse shaping, J. Mater. Process. Technol. 210 (2010) 279–287. https://doi.org/10.1016/j.jmatprotec.2009.09.011.

[12] K.A. Mumtaz, P. Erasenthiran, N. Hopkinson, High density selective laser melting of Waspaloy, J. Mater. Process. Technol. 195 (2008) 77–87. https://doi.org/10.1016/j.jmatprotec.2007.04.117.

[13] W. O'Neill, C. Sutcliffe, R. Morgan, K.K.B. Hon, Investigation of short pulse Nd: YAG laser interaction with stainless steel powder beds, Proc. SFF Symp. (1998). http://utwired.engr.utexas.edu/lff/symposium/proceedingsArchive/pubs/Manuscripts/1998/1998-15-ONeill.pdf.

[14] R. Morgan, C.J. Sutcliffe, W. O'Neill, Density analysis of direct metal laser re-melted 316L stainless steel cubic primitives, J. Mater. Sci. 39 (2004) 1195–1205. https://doi.org/10.1023/B:JMSC.0000013875.62536.fa.

[15] L. Caprio, A.G. Demir, B. Previtali, Influence of pulsed and continuous wave emission on melting efficiency in selective laser melting, J. Mater. Process. Tech. 266 (2018) 429–441. https://doi.org/10.1016/j.jmatprotec.2018.11.019.

[16] C.A. Biffi, J. Fiocchi, P. Bassani, A. Tuissi, Continuous wave vs pulsed wave laser emission in selective

laser melting of AlSi10Mg parts with industrial optimized process parameters: microstructure and mechanical behaviour, Addit. Manuf. 24 (2018) 639–646. https://doi.org/10.1016/j.addma.2018.10.021.

[17] A.E. Wilson-Heid, Z. Wang, B. McCornac, A.M. Beese, Quantitative relationship between anisotropic strain to failure and grain morphology in additively manufactured Ti-6Al-4V, Mater. Sci. Eng. A. 706 (2017) 287–294. https://doi.org/10.1016/j.msea.2017.09.017.

[18] J. Zhang, D.C. Weckman, Y. Zhou, Effects of temporal pulse shaping on cracking susceptibility of 6061-T6 aluminum Nd:YAG laser welds, Weld. J. (Miami, Fla). 87 (2008) 18–30.

[19] A.G. Demir, L. Mazzoleni, L. Caprio, M. Pacher, B. Previtali, Complementary use of pulsed and continuous wave emission modes to stabilize melt pool geometry in laser powder bed fusion, Opt. Laser Technol. 113 (2019). https://doi.org/10.1016/j.optlastec.2018.12.005.

[20] S.M.H. Hojjatzadeh, Q. Guo, N.D. Parab, M. Qu, L.I. Escano, K. Fezzaa, W. Everhart, T. Sun, L. Chen, In-situ characterization of pore formation dynamics in pulsed wave laser powder bed fusion, Materials (Basel). 14 (2021) 1–11. https://doi.org/10.3390/ma14112936.

[21] IPG Photonics fiber laser sources, (n.d.). https://www.ipgphotonics.com/en/products/lasers/mid-power-cw-fiber-lasers#[1-micron] (accessed June 7, 2022).

[22] Coherent fiber laser sources, (n.d.). https://www.coherent.com/lasers/fiber/highlight-fl (accessed June 7, 2022).

[23] nLight fiber laser sources, (n.d.). https://www.nlight.net/rackmount-fiber-lasers.

[24] O. Oreshkin, M. Küpper, A. Temmler, E. Willenborg, Active reduction of waviness through processing with modulated laser power, J. Laser Appl. 27 (2015) 022004. https://doi.org/10.2351/1.4906622.

[25] F.C. Neto, M.C. Fredel, M. Pereira, L.E. dos S. Paes, Laser power modulation to grain refinement of SAE 1045 steel welds, J. Laser Appl. 32 (2020) 022027. https://doi.org/10.2351/7.0000096.

[26] J. Ning, L.J. Zhang, L. liang Zhang, J. Long, X. qing Yin, J.X. Zhang, S.J. Na, Effects of power modulation on behaviours of molten pool and keyhole during laser–arc hybrid welding of pure copper, Mater. Des. 194 (2020) 108829. https://doi.org/10.1016/j.matdes.2020.108829.

[27] J. Ning, S.J. Na, L.J. Zhang, X. Wang, J. Long, W.I. Cho, Improving thermal efficiency and stability of laser welding process for magnesium alloy by combining power modulation and subatmospheric pressure environment, J. Magnes. Alloy. (2021). https://doi.org/10.1016/j.jma.2021.02.005.

[28] J. Gedicke, A. Olowinsky, J. Artal, A. Gillner, Influence of temporal and spatial laser power modulation on melt pool dynamics, 26th Int. Congr. Appl. Lasers Electro-Optics, ICALEO 2007 - Congr. Proc. 1502 (2007). https://doi.org/10.2351/1.5061009.

[29] L. Caprio, A.G. Demir, B. Previtali, Observing molten pool surface oscillations during keyhole processing in laser powder bed fusion as a novel method to estimate the penetration depth, Addit. Manuf. 36 (2020) 101470. https://doi.org/10.1016/j.addma.2020.101470.

[30] S.A. Khairallah, A.T. Anderson, A. Rubenchik, W.E. King, Laser powder-bed fusion additive manufacturing: Physics of complex melt flow and formation mechanisms of pores, spatter, and denudation zones, Acta Mater. 108 (2016) 36–45. https://doi.org/10.1016/j.actamat.2016.02.014.

[31] M. Xia, D. Gu, G. Yu, D. Dai, H. Chen, Q. Shi, Influence of hatch spacing on heat and mass transfer, thermodynamics and laser processability during additive manufacturing of Inconel 718 alloy, Int. J. Mach. Tools Manuf. 109 (2016) 147–157. https://doi.org/10.1016/j.ijmachtools.2016.07.010.

[32] J. Dowden, Why Construct Analytical Models Of Laser Welding?, in: AIP Conf. Proc., 2008: pp. 3–11.

[33] G. Simon, U. Gratzke, J. Kroos, Analysis of heat conduction in deep penetration welding with a time-modulated laser beam, J. Phys. D. Appl. Phys. 26 (1993) 862–869. https://doi.org/10.1088/0022-3727/26/5/022.

[34] A. Temmler, N. Pirch, J. Luo, J.H. Schleifenbaum, C.L. Häfner, Numerical and experimental investigation on formation of surface structures in laser remelting for additive-manufactured Inconel 718, Surf. Coatings Technol. 403 (2020) 126370. https://doi.org/10.1016/j.surfcoat.2020.126370.

[35] A. Temmler, D. Wei, T. Schmickler, M.E. Küpper, C.L. Häfner, Experimental investigation on surface structuring by laser remelting (WaveShape) on Inconel 718 using varying laser beam diameters and scan speeds, Appl. Surf. Sci. 541 (2021) 147814. https://doi.org/10.1016/j.apsusc.2020.147814.

[36] S. Pang, K. Hirano, R. Fabbro, T. Jiang, Explanation of penetration depth variation during laser welding under variable ambient pressure, J. Laser Appl. 27 (2015) 022007. https://doi.org/10.2351/1.4913455.

[37] T. Cullom, C. Lough, N. Altese, D. Bristow, R. Landers, B. Brown, T. Hartwig, A. Barnard, J. Blough, K. Johnson, E. Kinzel, Frequency domain measurements of melt pool recoil force using modal analysis, Sci. Rep. 11 (2021) 1–12. https://doi.org/10.1038/s41598-021-90423-z.

[38] N. Kouraytem, X. Li, R. Cunningham, C. Zhao, N. Parab, T. Sun, A.D. Rollett, A.D. Spear, W. Tan, Effect of Laser-Matter Interaction on Molten Pool Flow and Keyhole Dynamics, Phys. Rev. Appl. 11 (2019) 064054. https://doi.org/10.1103/PhysRevApplied.11.064054.

[39] H.S. Carslaw, J.C. Jaeger, Conduction of heat in solids, Clarendon Press, 1959.

[40] D. Rosenthal, Mathematical theory of heat distribution during welding and cutting, Weld. J. 20 (1941).

[41] D. Rosenthal, The Theory of Moving Sources of Heat and Its Application of Metal Treatments, Trans. ASME. 68 (1946) 849–866.

[42] H.E. Cline, T.R. Anthony, Heat treating and melting material with a scanning laser or electron beam, J. Appl. Phys. 48 (1977) 3895–3900. https://doi.org/10.1063/1.324261.

[43] T.W. Eagar, N.S. Tsai, Temperature fields produced by traveling distributed heat sources, Weld. J. 62 (1983) 346–355.

[44] M.F. Ashby, K.E. Easterling, The transformation hardening of steel surfaces by laser beams-I. Hypo-eutectoid steels, Acta Metall. 32 (1984). https://doi.org/10.1016/0001-6160(84)90175-5.

[45] S.S. Singh, D. Roy, R. Mitra, R. V. Subba Rao, R.K. Dayal, B. Raj, I. Manna, Studies on laser sintering of mechanically alloyed Al50Ti40Si10 composite, Mater. Sci. Eng. A. 501 (2009) 242–247. https://doi.org/10.1016/j.msea.2008.10.011.

[46] J.M. Dowden, The mathematics of thermal modeling: an introduction to the theory of laser material processing, CRC Press, 2001.

[47] A. V. Gusarov, Radiative transfer, absorption, and reflection by metal powder beds in laser powder-bed processing, J. Quant. Spectrosc. Radiat. Transf. 257 (2020) 107366. https://doi.org/10.1016/j.jqsrt.2020.107366.

[48] C.D. Boley, S.A. Khairallah, A.M. Rubenchik, Calculation of laser absorption by metal powders in additive manufacturing, Addit. Manuf. Handb. Prod. Dev. Def. Ind. 54 (2017) 507–517. https://doi.org/10.1201/9781315119106.

[49] S.S. Sih, J.W. Barlow, The prediction of the emissivity and thermal conductivity of powder beds, Part. Sci. Technol. 22 (2004) 427–440. https://doi.org/10.1080/02726350490501682.

[50] H.J. Jo, J.L. King, K. Blomstrand, K. Sridharan, Spectral emissivity of oxidized and roughened metal surfaces, Int. J. Heat Mass Transf. 115 (2017) 1065–1071. https://doi.org/10.1016/j.ijheatmasstransfer.2017.08.103.

[51] C.L.A. Leung, S. Marussi, M. Towrie, R.C. Atwood, P.J. Withers, P.D. Lee, The effect of powder oxidation on defect formation in laser additive manufacturing, Acta Mater. 166 (2019) 294–305. https://doi.org/10.1016/j.actamat.2018.12.027.

[52] A.F.H. Kaplan, Absorptivity modulation on wavy molten steel surfaces: The influence of laser wavelength

and angle of incidence, Appl. Phys. Lett. 101 (2012) 151605. https://doi.org/10.1063/1.4759126.

[53] J.M. Dowden, Mathematics Modeling Theory of Laser Material Processing, CRC Press, 2001.

[54] S.I. Anisimov, Vaporization of Metal Absorbing Laser Radiation, J. Exp. Theor. Phys. 27 (1968) 182–183. https://doi.org/10.1142/9789814317344_0002.

[55] C.J. Knight, Theoretical modeling of rapid surface vaporization with back pressure, AIAA J. 17 (1979) 519–523. https://doi.org/10.2514/3.61164.

[56] K.C. Mills, Recommended values of thermophysical properties for selected commercial alloys, Woodhead Publishing, 2002. https://doi.org/10.1533/9781845690144.

[57] C.S. Kim, Thermophysical properties of stainless steels, 1975.

[58] V. Semak, A. Matsunawa, The role of recoil pressure in energy balance during laser materials processing, J. Phys. D. Appl. Phys. 30 (1997) 2541–2552. https://doi.org/10.1088/0022-3727/30/18/008.

[59] J.Y. Lee, S.H. Ko, D.F. Farson, C.D. Yoo, Mechanism of keyhole formation and stability in stationary laser welding, J. Phys. D. Appl. Phys. 35 (2002) 1570–1576. https://doi.org/10.1088/0022-3727/35/13/320.

[60] S. Ly, G. Guss, A.M. Rubenchik, W.J. Keller, N. Shen, R.A. Negres, J. Bude, Resonance excitation of surface capillary waves to enhance material removal for laser material processing, Sci. Rep. 9 (2019) 1–9. https://doi.org/10.1038/s41598-019-44577-6.

[61] J. Yin, D. Wang, L. Yang, H. Wei, P. Dong, L. Ke, G. Wang, H. Zhu, X. Zeng, Correlation between forming quality and spatter dynamics in laser powder bed fusion, Addit. Manuf. 31 (2020) 100958. https://doi.org/10.1016/j.addma.2019.100958.

List of tables

List of figures

video n°2 which reports the recoil pressure variations at the different time instants. The colour scaling of temperature is limited at the vaporisation temperature of AISI316L to improve visualization of the temperature waves induced by the time-varying power input.

Figure 8. Estimated melt surface temperature and recoil pressure at different time instants at a specific position on the melt surface behind the laser material interaction corresponding to x=50 µm, y=5 µm, z= 0 µm for the different waveforms (a) Square, (b) Triangle, (c) Ramp Up and (d) Ramp Down with ΔP=400 W and f_w=2kHz. Dashed black line represents reference temperature estimated with CW emission.

Figure 9. Pressure distribution in the x-y field at a time instant of the simulation corresponding to $t=t_0$+500 µs for the different waveform shapes with ΔP=200W, f_w=2 kHz. The reader is referred also to supplementary video n°2 which reports the recoil pressure variations at the different time instants. The colour scaling of the pressure is limited at 10 MPa to enhance the visualisation.

Figure 10. Estimated melt surface temperature and recoil pressure at different time instants at a specific position on the melt surface behind the laser material interaction corresponding to x=50 µm, y=5 µm, z= 0 µm for different levels of waveform amplitude (ΔP=200 W for (a)-(d), ΔP=400 W for (e)-(h)), and waveform frequency for Square Wave.

Figure 11. Estimated melt surface temperature and recoil pressure at different time instants at a specific position on the melt surface behind the laser material interaction corresponding to x=50 µm, y=5 µm, z= 0 µm for different levels of waveform amplitude (ΔP=200 W for (a)-(d), ΔP=200 W for (e)-(h)), and waveform frequency for Triangle Wave.

Figure 12. Maximum temperature achieved in the different conditions simulated at the position x=50 µm, y=5 µm, z= 0 µm. Reference temperature from simulation of CW emission in dashed red line.